# Electronic Supplementary Information

## Experimental section

**Materials:** Fe foil (Fe) was obtained from Tianjin Fajiu metal material Co. Ltd., and pretreated in HCl for further application. Tetracyanoquinodimethane (TCNQ) was supported by Tianjin Fuyu Chemical Reagent Co. Ltd. Nafion (5 wt%) and $RuCl_3 \cdot 3H_2O$ were bought from Sigma-Aldrich Chemical Reagent Co., Ltd. Water used in all experiments was obtained from a Millipore purified system. All the reagents were used as received without further purification.

**Preparation of $Fe(TCNQ)_2$/Fe and $\alpha$-$Fe_2O_3$/Fe:** $Fe(TCNQ)_2$/Fe was prepared as follows. Firstly, dissolving TCNQ into pure acetonitrile in a 10 mL centrifuge tube under vigorous magnetic stirring for 15 min, forming a 7 mM TCNQ solution. Then, a piece of pre-cleaned Fe foil was immersed into the as-prepared solution and the centrifuge tube was sealed and maintained at 60 °C for 4 h in an electric oven. After the centrifuge tube cooled naturally to room temperature, the resulting Fe foil was taken out and cleaned with distilled water and ethanol several times, followed by drying at 60 °C for 6 h. TCNQ is an organic electron acceptor with an electron affinity of 2.88 eV. This allows TCNQ to react readily with transition metals that act as electron donors to form a myriad of TCNQ anion-based salt complexes (Catal. Today, 2016, 278, 319–329). When TCNQ in acetonitrile contacts the Fe foil, a direct oxidation-reduction reaction occurs spontaneously on the metal surface to form $Fe^{2+}$ and $TCNQ^-$ resulting in the formation of $Fe(TCNQ)_2$, finally. $\alpha$-$Fe_2O_3$/Fe was prepared by calcinating wettish Fe foil at 500 °C for 3 h in a muffle furnace.

**Synthesis of $RuO_2$:** In a typical synthesis,[1] 2.61 g of $RuCl_3 \cdot 3H_2O$ was dissolved into 100 ml distilled water and stirred for 10 min at 100 °C. Then 1.0 ml KOH (1.0 M) was added into the above solution and stirred for 45 minutes. The precipitates were collected and washed with distilled water several times, further dried at 80 °C overnight and then annealed at 300 °C in air atmosphere for 3 h. $RuO_2$ ink was prepared by dispersing 20 mg of catalyst into 490 μL of water/ethanol (v/v = 1:1) and 10 μL of 5 wt% Nafion using sonication for 30 min. Then 3.0 μL of the $RuO_2$ ink

(containing 0.12 mg of $RuO_2$) was loaded onto a bare Fe foil of 0.25 $cm^{-2}$ in geometric area (loading: 0.49 mg $cm^{-2}$).

**Characterizations:** XRD data were acquired from a LabX XRD-6100 X-ray diffractometer with Cu Kα radiation (40 kV, 30 mA) of wavelength 0.154 nm (SHIMADZU, Japan). SEM measurements were performed on a XL30 ESEM FEG scanning electron microscope at an accelerating voltage of 20 kV. XPS spectra were acquired on an ESCALABMK II X-ray photoelectron spectrometer using Mg as the exciting source.

**Electrochemical measurements:** Electrochemical measurements were performed with a CHI 660E electrochemical analyzer (CH Instruments, Inc., Shanghai) in a standard three-electrode system. $Fe(TCNQ)_2$/Fe was used as the working electrode, a graphite plate as the counter electrode and Hg/HgO as the reference electrode in KOH. The experimental temperature was kept at 25 °C for all electrochemical measurements. All the potentials were calibrated to RHE other than especially stated, following the equation: $E$ (RHE) = $E$ (Hg/HgO) + (0.098 + 0.059 $pH$) V.

**Tafel plots calculation:** The Tafel plots are employed to evaluate the OER catalytic kinetics and fitted with the following equation:

$$\eta = b \log j + a$$

Where j is the current density and b is the Tafel slope.

**Double layer capacitance ($C_{dl}$) measurements:** To measure the electrochemical capacitance, the potential was swept between +0.87 to +0.97 V vs. RHE at different scan rates (50, 100, 150, 200, 250 and 300 mV $s^{-1}$) with an assumption of double layer charging in the potential range. The capacitive currents at 0.92 V vs. RHE were measured and plotted as a function of scan rate.

**Determination of FE:** The oxygen generated at anode was measured quantitatively by using a calibrated pressure sensor to monitor the pressure change in the anode compartment of a H-type electrolytic cell. The FE was calculated by comparing the amount of experimentally measured oxygen generated by potentiostatic anodic electrolysis with theoretically calculated oxygen (assuming 100% FE). Pressure data

during electrolysis were recorded using a CEM DT-8890 Differential Air Pressure Gauge Manometer Data Logger Meter Tester with a sampling interval of one point per second.

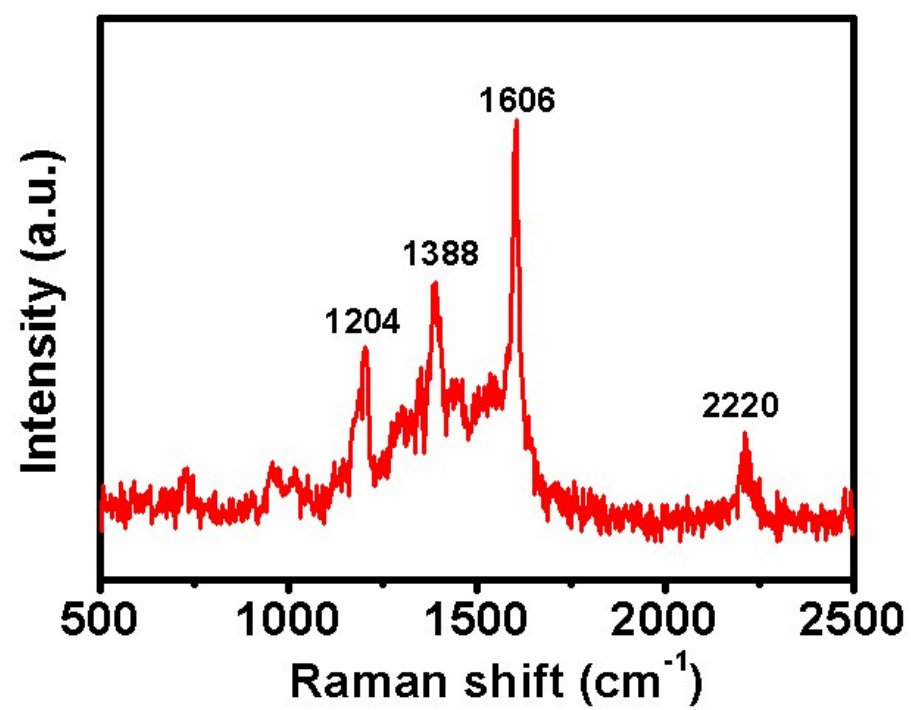


**Fig. S1.** Raman spectrum of $Fe(TCNQ)_2$.

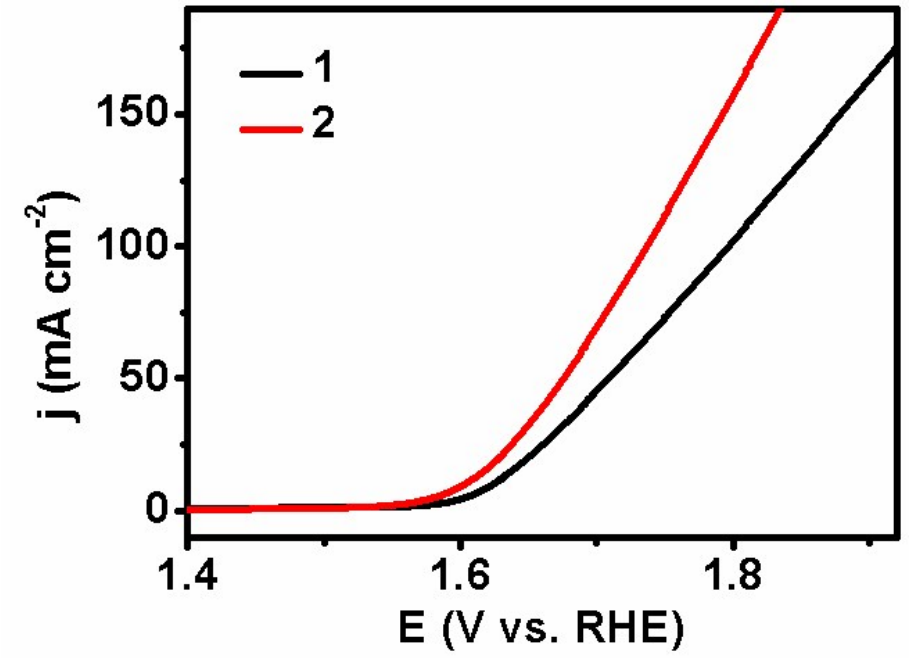


**Fig. S2.** LSV curves for $Fe(TCNQ)_2$ powder/GCE (curve 1) and $Fe(TCNQ)_2$ powder/Fe (curve 2) in 1.0 M KOH.

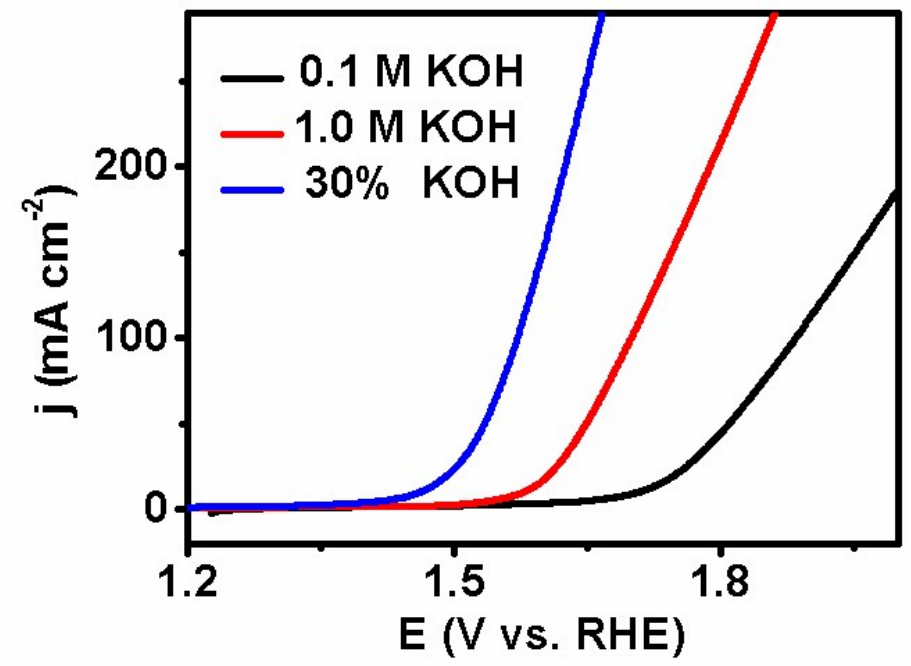


**Fig. S3.** LSV curves for $Fe(TCNQ)_2$/Fe in 0.1 M , 1.0 M and 30% KOH for OER.

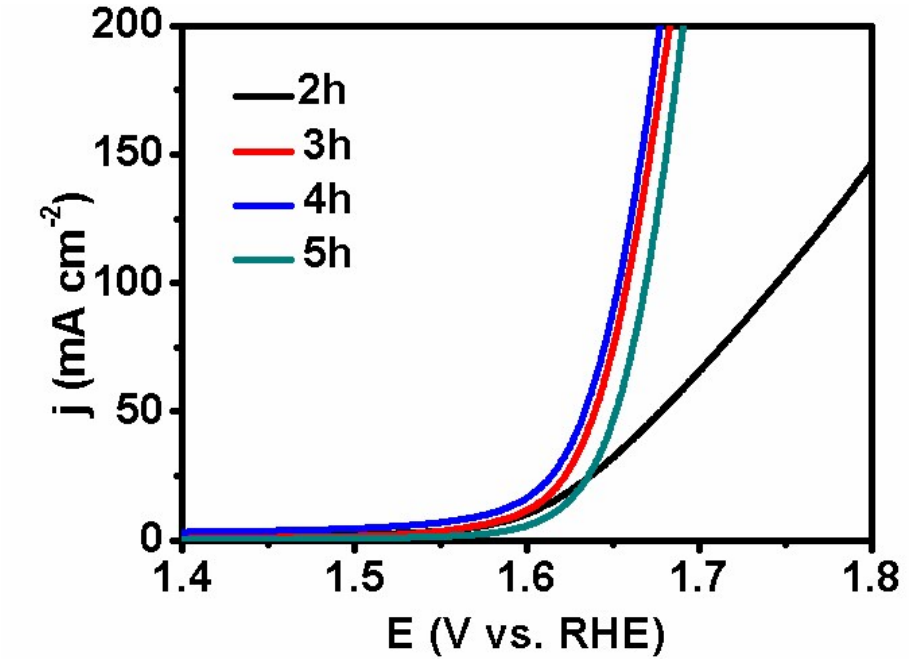


**Fig. S4.** LSV curves for $Fe(TCNQ)_2$/Fe synthesized with various immersion time for OER in 1.0 M KOH.

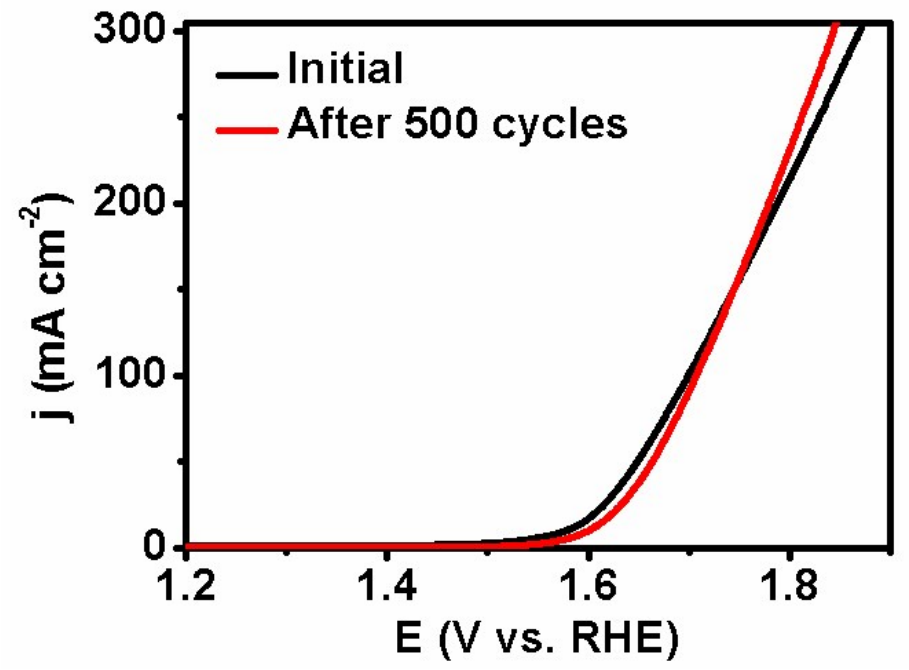


**Fig. S5.** LSV curves for $Fe(TCNQ)_2$/Fe before and after 500 cyclic voltammetry cycles.

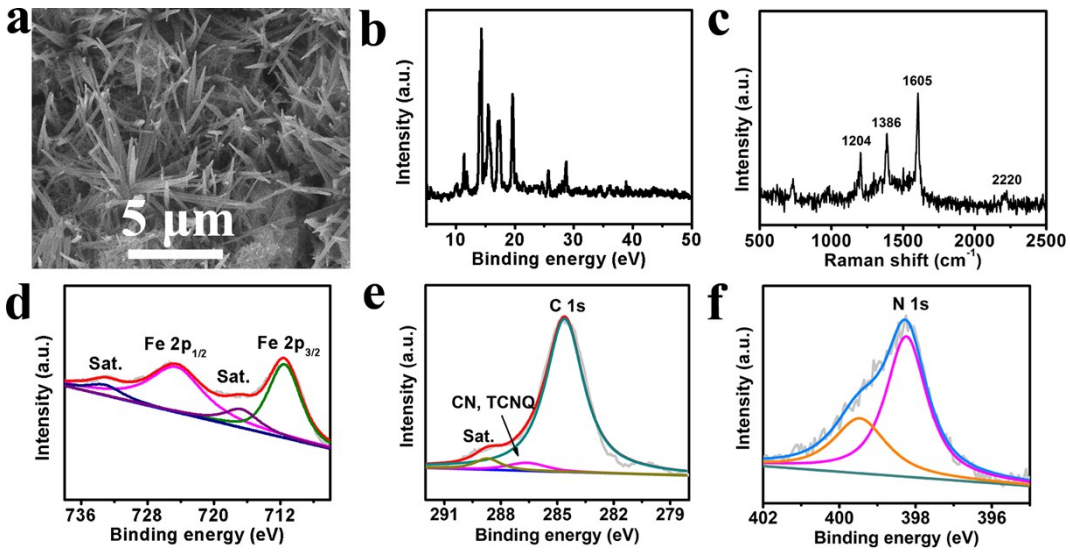


**Fig. S6.** (a) SEM image for $Fe(TCNQ)_2$/Fe after stability test. (b) XRD pattern for $Fe(TCNQ)_2$ after stability test. (c) Raman spectrum of $Fe(TCNQ)_2$, and XPS spectra for $Fe(TCNQ)_2$ in the (d) Fe 2p, (e) C 1s and (f) N 1s regions. All characterization was conducted after stability test.

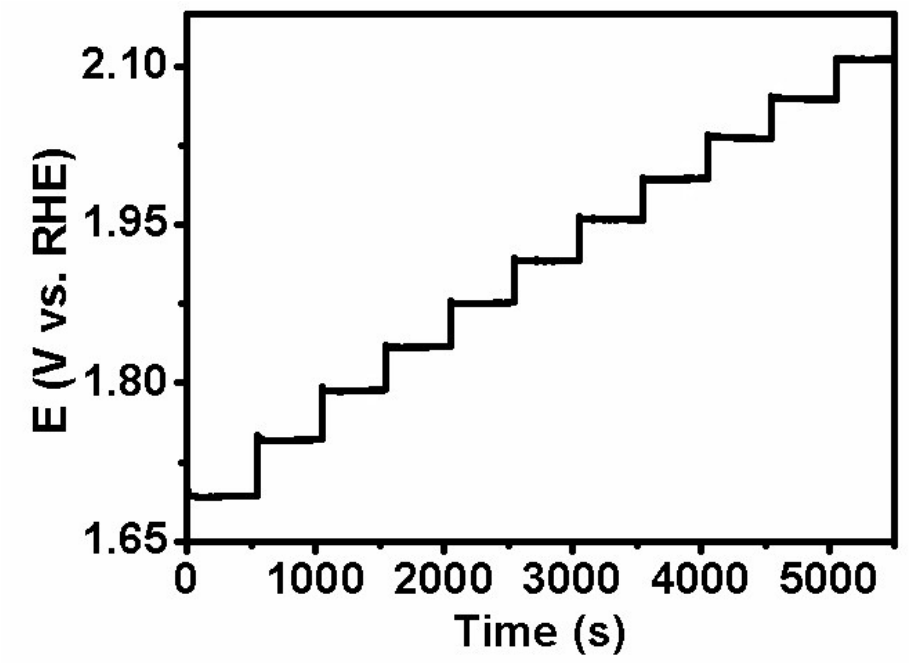


**Fig. S7.** Multi-step chronopotentiometric curve for $Fe(TCNQ)_2$/Fe. The current density started at 40 mA $cm^{-2}$ and ended at 440 mA $cm^{-2}$, with an increment of 40 mA $cm^{-2}$ per 500 s without iR correction.

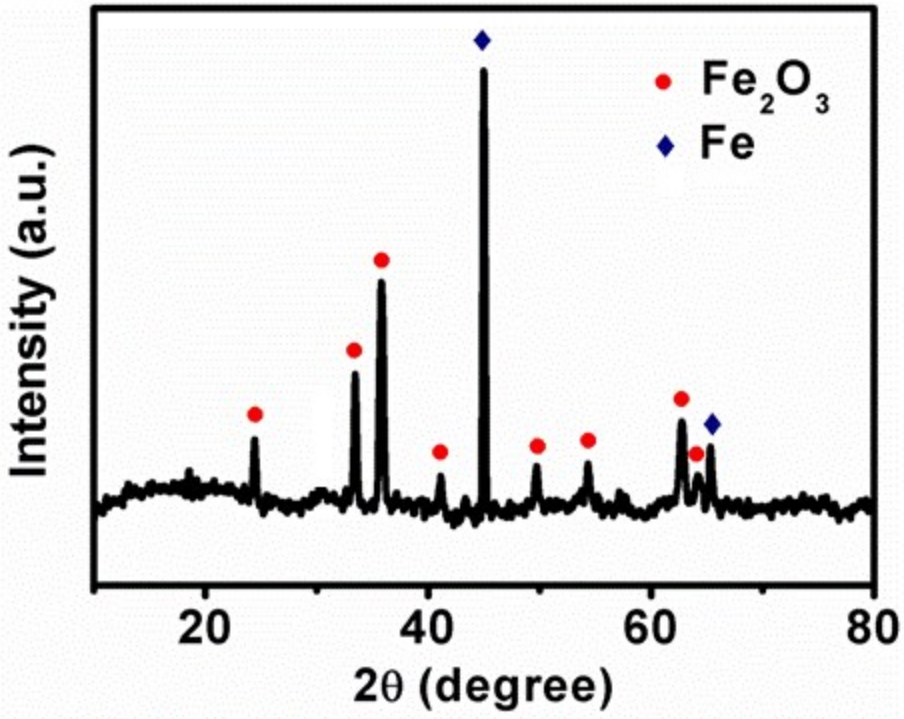


**Fig. S8.** XRD pattern for α-$Fe_2O_3$/Fe.

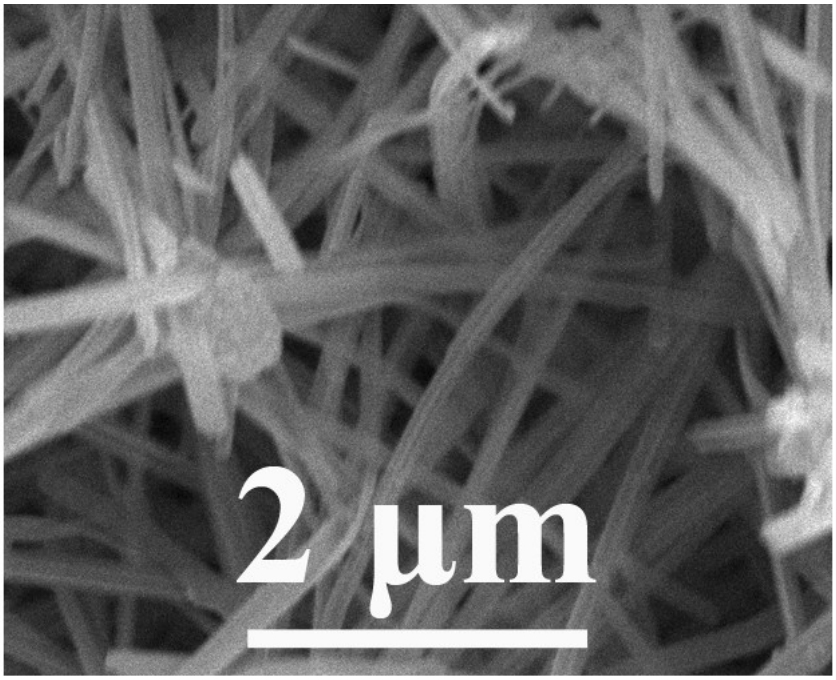


**Fig. S9.** SEM image for α-$Fe_2O_3$/Fe.

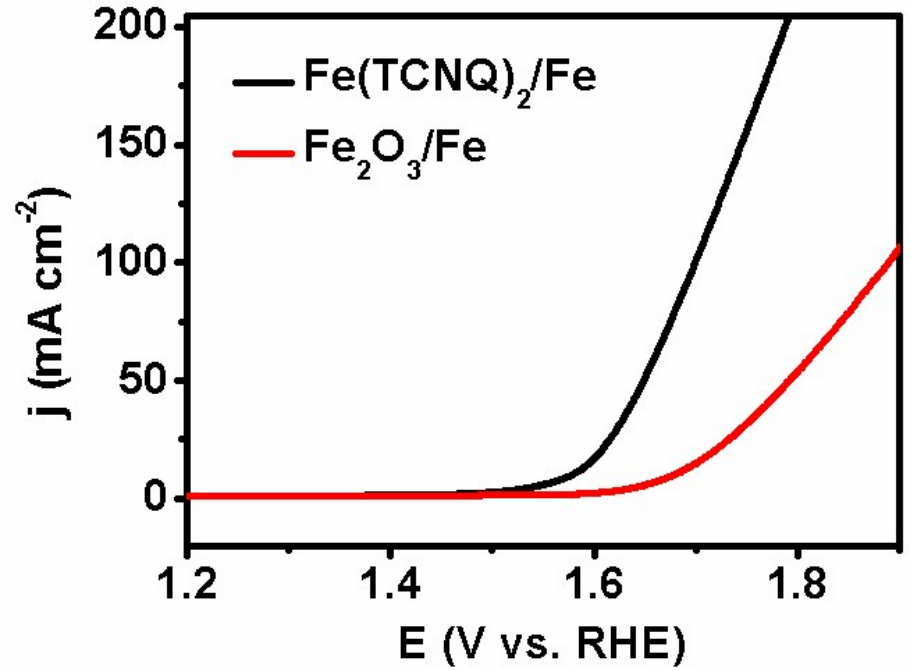


**Fig. S10.** LSV curves for $Fe(TCNQ)_2$/Fe and α-$Fe_2O_3$/Fe in 1.0 M KOH.

**Table S1.** Comparison of OER performance for $Fe(TCNQ)_2$/Fe with other non-noble-metal electrocatalysts in alkaline media.

| Catalyst | j(mA $cm^{-2}$) | $\eta$ (mV) | Electrolyte | Ref. |
|---|---|---|---|---|
| $Fe(TCNQ)_2$/Fe | 10 | 340 | 1.0 M KOH | This work |
| | 20 | 370 | 1.0 M KOH | |
| | 30 | 390 | 1.0 M KOH | |
| | 10 | 478 | 0.1 M KOH | |
| A-Fe film | 10 | 600 | 1.0 M KOH | 2 |
| α-FeOOH | 10 | ~490 | 1.0 M KOH | 3 |
| FeOOH2 | 10 | 530 | 0.1 M KOH | 4 |
| FeOOH NTAs-NF | 20 | ~350 | 1.0 M NaOH | 5 |
| Fe-$Co_3O_4$ nanocast | 10 | 486 | 0.1 M KOH | 6 |
| $Ni_{30}Fe_7Co_{20}Ce_{43}O_x$ | 10 | 410 | 1.0 M KOH | 7 |
| $Fe_{0.5}V_{0.5}$ spheres | 10 | 390 | 1.0 M KOH | 8 |
| mesoporous $Co_3O_4$ | 10 | 525 | 0.1 M KOH | 9 |
| reduced $Co_3O_4$ (0.136) | 10 | ~410 | 1.0 M KOH | 10 |
| Exfoliated NiCo-LDH | 10 | 367 | 1.0 M KOH | 11 |
| CoMn-LDH (0.142) | 10 | 350 | 1.0 M KOH | 12 |
| Co-S/Ti mesh | 10 | 361 | 1.0 M KOH | 13 |
| Co-P film | 10 | 345 | 1.0 M KOH | 14 |
| CoP-MNA/NF | 10 | 390 | 1.0 M KOH | 15 |
| Ni-$Co_2$-O | 10 | 362 | 1.0 M KOH | 16 |
| $Ni_{2.3\%}$–$CoS_2$/CC | 100 | 370 | 1.0 M KOH | 17 |
| Ni–Co–S/CF | 100 | 363 | 1.0 M KOH | 18 |
| Hollow $Fe_{0.5}V_{0.5}$ spheres | 10 | 390 | 1.0 M KOH | 19 |
| 2D CuO nanosheet | 10 | 350 | 1.0 M KOH | 20 |
| NiCo LDHs | 10 | 367 | 1.0 M KOH | 21 |

| | | | | |
|---|---|---|---|---|
| Co@CoO | 10 | 350 | 1.0 M KOH | 22 |
| $CoO_x$ | 10 | 390±40 | 1.0 M KOH | 23 |
| $Cu_xCo_yO_4$ | 10 | 391 | 1.0 M KOH | 24 |

**References**


1 J. C. Cruz, V. Baglio, S. Siracusano, V. Antonucci, A. S. Aricò, R. Ornelas, L. Ortiz-Frade, G. Osorio-Monreal, S. M. Durón-Torres and L. Arriaga, *Int. J. Electrochem. Sci.,* 2011, **6**, 6607–6619.

2 D. R. Chowdhury, L. Spiccia, S. S. Amritphale, A. Paul and A. Singh, *J. Mater. Chem. A*, 2016, **4**, 3655–3660.

3 W. Luo, C. Jiang, Y. Li, S. A. Shevlin, X. Han, K. Qiu, Y. Cheng, Z. Guo, W. Huang and J. Tang, *J. Mater. Chem. A,* 2017, **5**, 2021–2028.

4 X. Zhang, L. An, J. Yin, P. Xi, Z. Zheng and Y. Du, *Sci. Rep.,* 2017, **7**, 43590.

5 J. Feng, H. Xu, Y. Dong, S. Ye, Y. Tong and G. Li, *Angew. Chem., Int. Ed.,* 2016, **55**, 3694–3698.

6 T. Grewe, X. Deng and H. Tüysüz, *Chem. Mater.,* 2014, **26**, 3162–3168.

7 J. A. Haber, Y. Cai, S. Jung, C. Xiang, S. Mitrovic, J. Jin, A. T. Bell and J. M. Gregoire, *Energy Environ. Sci.,* 2014, **7**, 682–688.

8 C. Tang, N. Cheng, Z. Pu, W. Xing and X. Sun, *Angew. Chem., Int. Ed.,* 2015, **54**, 9351–9355.

9 H. Tüysüz, Y. J. Hwang, S. B. Khan, A. M. Asiri and P. Yang, *Nano Res.,* 2013, **6**, 47–54.

10 Y. Wang, T. Zhou, K. Jiang. P. Da, Z. Peng, J. Tang, B. Kong, W-B. Cai, Z. Yang and G. Zheng, *Adv. Energy Mater.,* 2014, 1400696.

11 H. Liang, F. Meng, M. Cabán-Acevedo, L. Li, A. Forticaux, L. Xiu, Z. Wang and S. Jin, *Nano Lett.,* 2015, **15**, 1421–1427.

12 F. Song and X. Hu, *J. Am. Chem. Soc.,* 2014, **136**, 16481–16484.

13 T. Liu, Y. Liang, Q. Liu, X. Sun, Y. He and A. M. Asiri, *Electrochem. Commun.,* 2015, **60**, 92–96.

14 N. Jiang, B. You, M. Sheng and Y. Sun, *Angew. Chem., Int. Ed.,* 2015, **54**, 6251–6254.

15 Y. Zhu, Y. Liu, T. Ren and Z. Yuan, *Adv. Funct. Mater.,* 2015, **25**, 7337–7347.

16 C. Zhu, D. Wen, S. Leubner, M. Oschatz, W. Liu, M. Holzschuh, F. Simon, S.

Kaskel and A. Eychmüller, *Chem. Commun.,* 2015, **51**, 7851–7854.

17 W. Fang, D. Liu, Q. Lu, X. Sun and A. M. Asiri, *Eletrochem. Commun.,* 2016, **63**, 60–64.

18 T. Liu, X. Sun, A. M. Arisi and Y. He, *Int. J. Hydrogen Energy,* 2016, **41**, 7264–7269.

19 K. Fan, Y. Ji, H. Zou, J. Zhang, B. Zhu, H. Chen, Q. Daniel, Y. Luo, J. Yu and L. Sun, *Angew. Chem., Int. Ed.,* 2017, **56**, 3289–3293.

20 S. M. Pawar, B. S. Pawar, B. Hou, J. Kim, A. T. A. Ahmed, H. S. Chavan, Y. Jo, S. Cho, A. I. Inamdar, J. L. Gunjakar, H. Kim, S. Cha and H. Im, *J. Mater. Chem. A,* 2017, **5**, 12747–12751.

21 H. Liang, F. Meng, M. Cabán-Acevedo, L. Li, A. Forticaux, L. Xiu, Z. Wang and S. Jin, *Nano Lett.,* 2015, **15**, 1421–1427.

22 S. Zhang, X. Yu, F. Yan, C. Li, X. Zhang and Y. Chen, *J. Mater. Chem. A,* 2016, **4**, 12046–12053.

23 C. C. L. McCrory, S. Jung, J. C. Peters and T. Jaramillo, *J. Am. Chem. Soc.,* 2013, **135**, 16977–16987.

24 T. Grewe, X. Deng, C. Weidenthaler, F. Schüth and H. Tüysüz, *Chem. Mater.,* 2013, **25**, 4926–4935.